Influence of particle size distribution on carbonbased flowable electrode viscosity and desalination efficiency in flow electrode capacitive deionization

Myriam Tauk, Mikhael Bechelany, Serge Lagerge, Philippe Sistat, Roland Habchi, Marc Cretin, Francois Zaviska

Influence of particle size distribution on carbon-based flowable electrode viscosity and desalination efficiency in flow electrode capacitive deionization.

Myriam Tauk, Mikhael Bechelany*, Serge Lagerge, Philippe Sistat, Roland Habchi, Marc Cretin and Francois Zaviska*

Institut Européen des Membranes, IEM, UMR-5635, University of Montpellier, ENSCM, CNRS, Place Eugène Bataillon, CEDEX 5, 34095 Montpellier, France;
myriam.tauk@umontpellier.fr (MT); mikhael.bechelany@umontpellier.fr (MB); serge.lagerge@umontpellier.fr (SL); philippe.sistat@umontpellier.fr (PS); rhabchi@ul.edu.lb (RH); marc.cretin@umontpellier.fr (MC); francois.zaviska@umontpellier.fr (FZ)
* Correspondance: marc.cretin@umontpellier.fr (MC), mikhael.bechelany@umontpellier.fr (MB), francois.zaviska@umontpellier.fr (FZ)

Abstract

Flow-electrode capacitive deionization (FCDI) is a potential energy-efficient electrochemical water desalination technology that combines ion-exchange membranes and flowable electrodes (FE). The performance of activated carbon (AC)-based FEs in FCDI systems is influenced by various factors, including particle size. Here, particle size commercial AC was reduced by dry ball milling to produce FEs for FCDI. Physical analysis by scanning electron microscopy and particle size analyzer confirmed the particle size reduction after dry ball milling. Then, the effect of particle size distribution on the rheological behavior and desalination performances of AC-based FEs was investigated by desalination performance indicators, such as desalination efficiency, average salt adsorption rate and charge efficiency. FE samples were prepared using different mixtures of fine-size range (0.65-0.92 µm; fine AC, FAC) and large-size range (1.5-2.3 µm; AC) particles. The AC to FAC particle ratio influenced the rheological properties of AC-based FEs in FCDI. Bimodal mixtures with 75% of FAC and 25% of AC (0.75:0.25 FAC:AC) particles displayed the highest desalination efficiency compared with pure AC and pure FAC FEs (72% *versus* 34% and 71%, respectively). Moreover, in our FCDI set-up, 0.75:0.25 FAC:AC bimodal mixtures showed better flowing properties than the pure FAC FEs, characterized by high viscosity.

Keywords: Flow electrode capacitive deionization, activated carbon flow electrode, particle size distributions, rheology, stability and desalination.

Graphical abstract

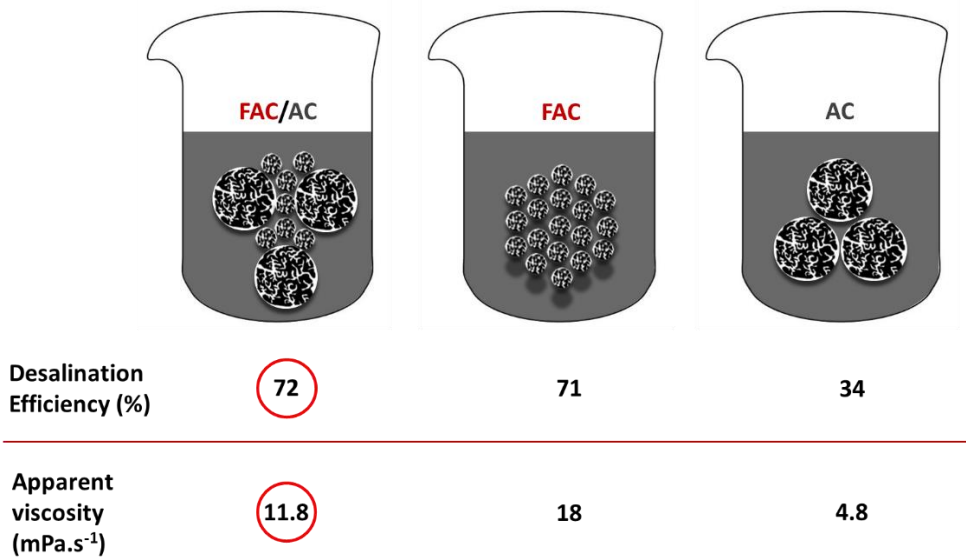

1. Introduction

Capacitive deionization (CDI) is used to eliminate charged species from water with various applications, such as brackish and sea water desalination, [1, 2] water softening,[3] and wastewater remediation.[4] CDI is an energy-efficient, cost-effective, and ecofriendly technology.[5] The first and most widely-used CDI set-up requires two porous carbon electrodes separated by a spacer through which water flows perpendicularly to the applied electric field.[5] In membrane CDI (MCDI), a key variation of the basic CDI set-up[6], the feed water flows between an anion exchange membrane at the anode and a cation exchange membrane at the cathode.[7] The membrane main role is to reduce co-ion adsorption. This improves the charge efficiency and can increase the charge storage in the electrode porous structure.[8] In the last decade, a new MCDI-based approach was developed to introduce carbon-based flowable electrodes.[9] The basis of this technology, called flow-electrode CDI (FCDI), is similar to that of electrochemical flow capacitors[10]. The process is based on electrical double layers that are formed on interfaces between porous activated carbon (AC)-based electrodes and an electrolyte (e.g. NaCl solution).[11] Ions are adsorbed and stored in the electrical double layers when a cell voltage in the range of 1–1.2 V is applied to the cell[12]. FCDI has three major advantages compared with other CDI systems. First, the continuous desalination of the feed water flowing through a single cell does not require an in situ discharge step for regenerating the ion-saturated AC-based electrodes, which is done in a separate process. This allows the easy scaling-up of FCDI[13]. Second, the continuous inflow of uncharged carbon particles into the charging cell increases the capacitance, which is needed for desalination, above that of static-electrode CDI systems.[14] This offers more flexibility because the desalination rate and kinetics can be easily controlled by adjusting the saline solution, flow electrode retention time, and the applied current charge. Third, in AC-based flowable electrodes, pores are more exposed and easily accessible for ion adsorption.

The choice of electrode material is a crucial factor in CDI system performance. The ideal CDI electrode material should meet the following criteria: 1) large specific surface area, high ion

adsorption sites; 2) high conductivity and ion mobility; 3) hydrophilicity to ensure full contact between the electrode porous structure and water; 4) electrochemical stability at different pH and voltages to ensure the system reliability and sustainability; 5) easily shapeable in function of the design requirements and economically feasible (i.e. availability, cost, and recyclability) for industrial development. Carbon-based materials are mostly used in this field because they meet these requirements. Moreover, to improve the properties of the carbon-based materials used as CDI electrodes, many methods have been tested and many carbon forms have been exploited, for instance AC, AC fibers, carbon aerogels, AC cloths,[15,16] carbon nanotubes,[17] graphene,[18] carbon nanofibers,[19] carbon sheet[20].

Porous AC, a cheap, easily available and reusable material, is widely used to prepare flowable electrodes for FCDI.[21] The electrochemical performance of AC-based flowable electrodes is influenced by several parameters, including mass loading, particle size and morphology, specific surface area, surface charge, viscosity, and hydrophilicity.[22] However, they display low wettability, pore inaccessibility for ions, and low conductivity. Therefore, to improve its features and overcome some of its limitations, AC can undergo physical or chemical treatments. For instance, pores can be expanded using physical treatments, such as thermal modification using inert gases (e.g. N_2, Ar, CO_2).[23] Surface area can be improved by exposure to KOH or NaOH followed by thermal treatment.[24] Much research has been done on hierarchical porous carbons with interconnected micro-mesopores for increasing ion adsorption.[25] Recent studies have investigated the particle size effect on the desalination performance of AC-based electrodes in CDI.[26] Cohen *et al.* combined dilute slurry electrodes and dense fluidized bed electrodes for better electric conductivity and lower resistance.[27] Zhang *et al.* found that AC-based electrodes with different particle sizes provide different CDI performances. Particularly, a mixture of large and small particles gave the best desalination performance in CDI.[26] However, the effect of particle size distribution on the viscosity and desalination performance of carbon slurry electrodes in FCDI has not been investigated yet. In a previous study, we found that reducing AC particle size in flowable electrodes can double the desalination rate in FCDI.[28] This was attributed to the enhanced connectivity between particles that increases charge transport and storage, thus improving conductivity through the AC percolating network. Moreover, in AC-based electrodes with finer particles, obtained by grinding, pores were more exposed, leading to faster ionic diffusion.[28] However, viscosity was increased upon particle size reduction. As the flowable electrode must flow along a narrow channel in the FCDI set-up, its rheological features are a crucial factor for limiting pressure drops and ensuring the absence of clogging. Indeed, the higher viscosity of the flowable electrode with fine AC particles, compared with normal AC particles, led to pumping and flowing difficulties inside the FCDI system. Therefore, in the present study, we wanted to decrease the viscosity of AC-based flowable electrodes, while maintaining the good desalination performance obtained with fine AC particles. To this aim, we mixed two AC particle size ranges to produce flowable electrodes for FCDI. We prepared bimodal slurries with different ratios of fine AC (FAC) to AC particles with the same carbon loading (10%) and characterized their rheological properties and desalination performance to find the best compromise between these parameters.

Our AC modification strategy for desalination improvement in FCDI is very simple, compared with the complex physical and chemical AC modifications that have been recently used in CDI. This is important, especially due to the major improvements in FCDI desalination efficiency

and viscosity reduction observed with these bimodal flowable electrodes compared with pure AC and FAC flowable electrodes.

2. Experimental

2.1. Material preparation

Commercial AC (Darco; CAS no: 7440-44-0) and sodium chloride (NaCl, CAS no: 7647-14-5, MW 58.44 g mol-1, 99%) were purchased from Sigma Aldrich. Cationic and anionic exchange membranes were purchased from Membranes International Inc. (Ringwood, New Jersey, USA). Deionized water (18 MΩ cm^{-2}) was prepared using a purification system.

AC powder was dry ball-milled using 50-mm diameter balls (350 rpm rotation speed) at room temperature for 90 minutes to obtain finer particles (

FE (10 % wt)	**AC (% wt)**	**FAC (% wt)**	**[NaCl] (g/L) (V=70 mL)**
FE1	10	0	1
FE2	8	2	1
FE3	5	5	1
FE4	2.5	7.5	1
FE5	0	10	1

)**Erreur ! Source du renvoi introuvable.**.[28] Ball-milled AC, called fine particle AC (FAC), and pristine AC with different particle size ranges (0.3-0.6 µm and 0.8-1.6 µm, respectively) were used for this study.

AC suspensions, used as flowable electrodes, were prepared by mixing the desired amounts of AC and FAC (10% wt as total weight percentage in each electrode) in 1 g/L NaCl solution (**Erreur ! Source du renvoi introuvable.**). Two different packing characteristics were chosen; i) monomodal distribution, where slurry electrodes contained only one particle size range (AC or FAC), and ii) bimodal distribution where slurry electrodes were mixtures of AC and FAC at different ratios. Then, the mixtures were sonicated for 2 h and stirred for 1 h to obtain a uniform particle distribution in suspension. The slurry electrode in a beaker was continuously stirred and was fed into the cell throughout the FCDI experiments (repeated three times for each sample).

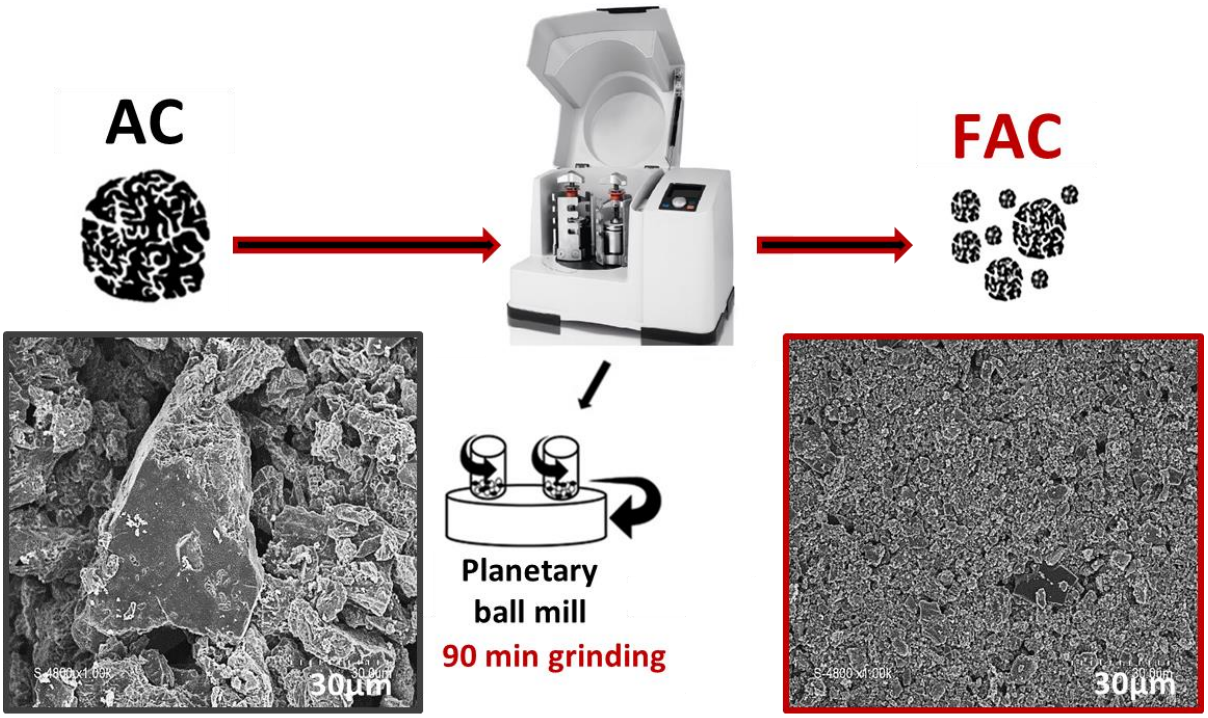

Figure 1: Planetary dry ball milling of activated carbon (AC) into fine activated carbon (FAC).

Table 1: Composition of the flowable electrodes (FE) used in this study

FE (10 % wt)	AC (% wt)	FAC (% wt)	[NaCl] (g/L) (V=70 mL)
FE1	10	0	1
FE2	8	2	1
FE3	5	5	1
FE4	2.5	7.5	1
FE5	0	10	1

2.2. AC Material Characterization

For all sample characterizations, carbon suspensions prepared in 1 g/L NaCl solution (experimental conditions) were used. Our previous study included a detailed physical characterization of AC and FAC (after grinding) samples[28]. AC and FAC particle size distribution and their zeta potentials were measured by dynamic light scattering using a Litesizer 500 particle size analyzer (Anton Paar, France). The particle structure was analyzed by scanning electron microscopy (SEM) (SEM, Hitachi S4800, Tokyo, Japan), and the atomic composition (chemical moieties) of the material was studied before and after ball milling (analyzed surface area = 300 x 700 µm) by X-ray photonelectron spectroscopy (XPS) (Spectrometre XPS/UPS KRATOS AXIS Ultra DLD). The surface area was measured using N_2 adsorption/desorption at 77 K. The specific surface area was calculated using the Brunauer-Emmett-Teller method (Micromeritics 2020 ASAP, Merignac France). The total pore volume (V_t) was calculated from the amount of N_2 adsorbed at 0.99 relative pressure (P/P_0). The

mesopore volume (V_{meso}) was calculated with the Barrett-Joyner-Halenda model. The dynamic viscosity of the different carbon suspensions (flow electrodes) was measured using a Paar Physica UDS 200 Rheometer, a concentric cylinder adapted for heterogeneous solutions or water suspensions, as a function of the shear rate at 25 °C. Dynamic viscosity describes the resistance of a liquid solution to flow, whereas the shear rate is the deformation speed of the suspension under an applied force. The physical stability or sedimentation rate of the different AC slurries over time was measured with a Formulaction TURBISCAN® in which static multiple light scattering is used to monitor particle migration in liquids. A measurement head with two detectors moves along the cell height to measure the transmission (T) and backscattering (BS) signals that are related to particle size and concentration in the sample. The changes over time are a sign of destabilization that is quantified using the TURBISCAN® stability index (TSI). Each experiment was repeated three times for each electrode type. The electrochemical properties of AC and FAC were tested by cyclic voltammetry (CV) method. CV tests were performed using Origalys OrigaStat OGS080 potentiostat and 3 electrodes system with a 5 mm carbon glass rotating disk electrode (RDE) as working electrode while a platinum mesh and a saturated 3 M KCl, Ag/AgCl electrode served as counter and reference electrodes respectively. 10% wt. activated carbon suspensions were prepared, 100 µl were deposited on the surface of the RDE then dried at 80°C before adding one drop of nafion ink to hold the material on the electrode. Voltammetry measurements were performed at a -0.2 V-0.4 V vs ref operating potential window in 5 g/L NaCl solution as electrolyte. The electrical double layer capacitance (EDLC) was determined using cyclic voltammetry cycles at 0.02 V. s^{-1} scan rate.

2.3. FCDI experiments

Figure 2 shows the FCDI experimental set-up and its operating principle. The system was composed of a homemade FCDI cell, a potentiostat (Origalys Electrochem, Origaflex), a conducti-meter (HANNA Instruments) to monitor the saline solution conductivity during the desalination experiment, and two beakers (one for the flowable electrode and the other for the saline solution) with two peristaltic pumps to recirculate both solutions through the electrochemical cell. Experiments were performed in a closed loop reactor at 1V constant voltage, using 5g/L NaCl as feed solution (FS), and lasted 30 min. The FDCI cell (**Erreur ! Source du renvoi introuvable.**(a)), specifically designed for these experiments, was composed of two current collectors (0.9mm depth, 8.5 cm width, and 14.5 cm length) with two channels each as flow electrode inflow and outflow of 7.8 cm depth, two ion exchange membranes (IEM) of 142 cm^2 effective area, a spacer (0.9 mm thick), two stainless steel plates, and nails to hold all parts together.

The electrical field created inside the FCDI cell drives ions present in the FS (5 g/L NaCl) through a spacer, sandwiched between two IEM, to be electrostatically attracted to the charged flowable electrodes that circulate through the flow paths carved on the current collectors, as shown in **Erreur ! Source du renvoi introuvable.**(a). When the flowable electrodes exit the channels, they are fed back into the reservoir, stirred, and then re-circulated inside the cell. The resulting current at the electrodes was monitored throughout the experiment by chronoamperometry. The FS and flowable electrodes were flowing at a constant flow rate of 3 $ml.min^{-1}$ and 40 $ml.min^{-1}$ respectively. Throughout the process, the conductivity of the FS that was recirculated in a closed loop system was monitored at room temperature with a

conductimeter (Hannah Instrument), as depicted in **Erreur ! Source du renvoi introuvable.**(b). To mention that no significant water transmembrane migration was observed during the desalination experiments.

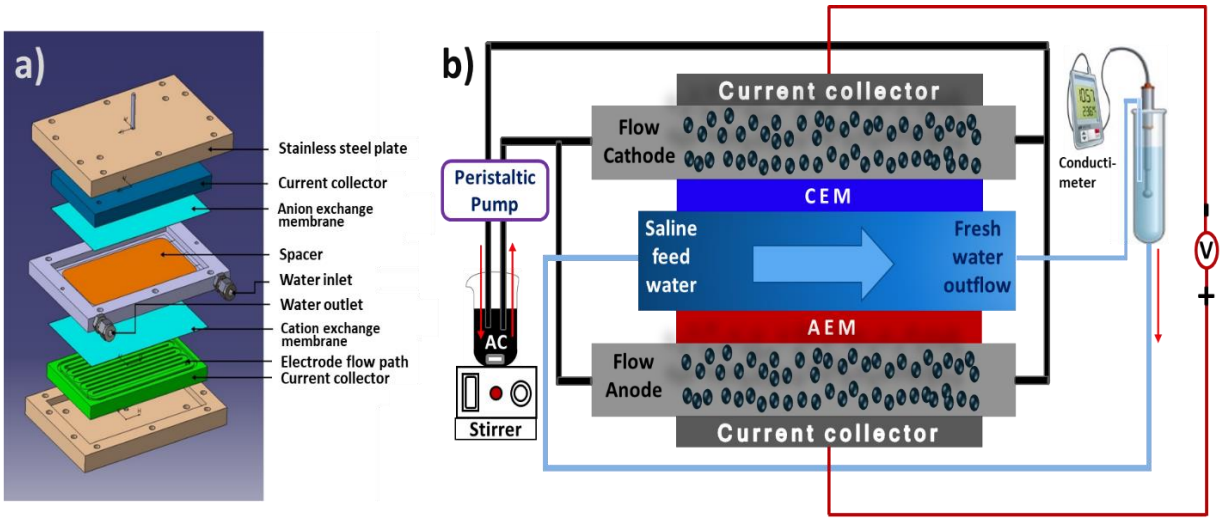

Figure 2: (a) FCDI cell. (b) Experimental set-up and operating principle. CEM: cationic exchange membrane; AEM: anionic exchange membrane

FCDI desalinating performance indicators were calculated for each experiment.

Salt adsorption capacity (SAC) indicating the mass of adsorbed salt as function of the adsorbent electrode weight is calculated according to equation (1) and expressed in mg of salt adsorbed per g of electrode material:

$$SAC = \frac{(C_0 - C_f)\,V}{m_{electrode}} \quad (1)$$

Where C_0 is the initial solute concentration of the feed solution, C_f the final solute concentration, V is the volume of the feed solution and $m_{electrode}$ is the mass of the electrode material.[29]

The salt removal efficiency or desalination efficiency (DE) was calculated using equation (2):

$$DE = \frac{(C_0 - C_f)}{C_0} \quad (2)$$

where C_0 and C_f are the initial and final concentrations (mol. L^{-1}) of the FS.[1]

The salt adsorption rate (SAR), which represents the amount of salt adsorbed (µg) per electrode surface (cm^2) per unit of time (min), was calculated using equation (3):

$$SAR\ (\mu g.cm^{-2}.min^{-1}) = \frac{(C_0 - C_f)\,V}{A\,t} \quad (3)$$

where V is the volume of the feed solution (L), A is the contact area between the feed electrode and the current collector, and t is the charging time.[30]

The charge efficiency (CE) or faradaic efficiency is the ratio of the electrical charges related specifically to ion removal over the total electrical charge applied by the potentiostat. It represents the energy efficiency of the system and was calculated using equation (4):

$$CE = \frac{z\,(C_0 - C_f)\,V\,F}{\int I dt} \quad (4)$$

where z is the equivalent charge of ions, V is the FS volume, F is the Faradaic constant, and $\int I dt$ is the integrated quantity of charge passed to the system over time.[31]

The Reynolds number shows the electrode flowing nature in the channel and was calculated with equation (5):

$$Re = \frac{\rho\,v\,D}{\eta} \quad (5)$$

where ρ and v are the flowable electrode density and velocity, respectively, in the flow channel calculated from the flow rate of the flowable electrode (0.0024 $m^3\ h^{-1}$) to the area of the flow cell (5.4 x 10^{-6} m^2), D is the hydraulic diameter of the flow channel (6 mm), and η is the mean coefficient of dynamic viscosity of the flowable electrode in function of the shear rate at 25 °C.

Stokes's law of sedimentation shows the drag force resisting the fall of small particles through a fluid medium under the influence of gravity, and is described by equation (6):

$$V = \frac{2\,(\rho_p - \rho_f)}{9\,\eta}\,g\,R^2 \quad (6)$$

where ρ_p is the particle density, ρ_f is the fluid density, g is the acceleration of gravity, R is the particle radius, and η is the viscosity.[32]

The linear pressure drop is the loss of mechanical energy caused by friction on the common walls of the network. It is directly affected by the fluid viscosity, and is described by equation (7):

$$\Delta P = \mu \frac{L}{D} \frac{1}{2} \rho v^2 \quad (7)$$

where μ is the friction coefficient with $\mu = 64/Re$, L and D are the canal length and diameter, ρ is the fluid apparent density, and v its velocity.[33]

The electrical double-layer capacitance (EDLC) was calculated according to equation (8):

$$C_{EDL} = \frac{\int I dV}{2\, u\, A\, \Delta V} \quad (8)$$

where C_{EDL} is the double layer capacitance, I is the current response, ΔV is the potential window, A is the effective area, and u is the scan rate.[34]

3. Results and discussion

3.1. Particle size reduction

AC and FAC morphological and structural properties were investigated in our previous study.[28] The dynamic light scattering (DLS) data (**Erreur ! Source du renvoi introuvable.** (a)) showed the difference in particle size distribution between pristine AC and FAC samples: 0.8-1.6 µm versus 0.3 to 0.6 µm respectively.

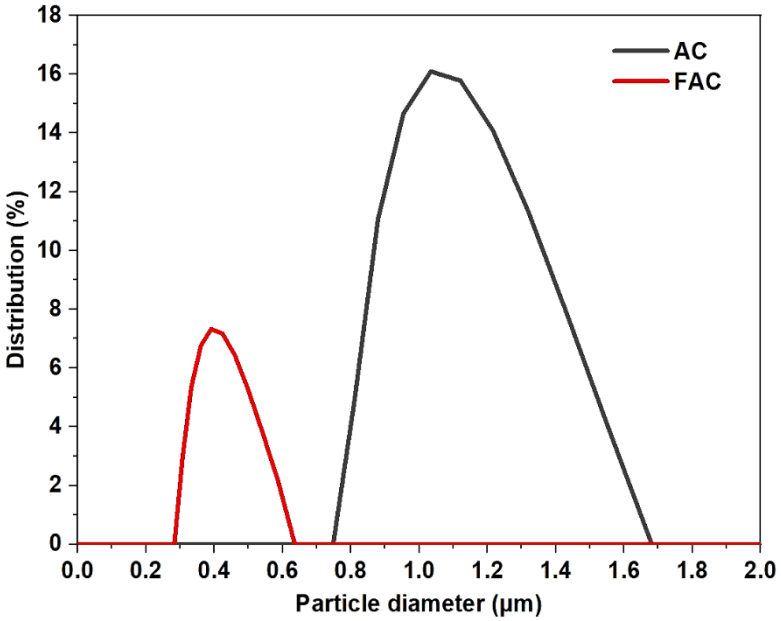

Figure 3: particle size distribution of AC and FAC after ball-milling measured by DLS method

3.2. Structural and textural characteristics

The structural and textural characteristics as well as the chemical moieties and composition of AC and FAC samples were described in our previous study and are summarized in Figure S1,

Table S1 and Figure S2 in supplementary information. Briefly, all AC characteristics were maintained in FAC after dry ball grinding, without any significant difference in texture (pores structure and surface area).[28]

3.3. Physical and chemical properties

3.3.1. Atomic composition

The atomic composition of the carbon material before and after ball milling was investigated using XPS. No band reduction was observed after ball milling. However, according to XPS analysis, the O1s atomic percentage of the carbon material slightly increased after ball milling from 5.10 % (AC) to 5.25 % (FAC), which can be due to the generation of new oxygenated surface functional groups after ball milling. Figure 4 a shows the complete spectra of both AC and FAC, while c and d present the resolved C 1s spectrum of AC and FAC respectively into their individual peaks. 284.00, 284.80 and 286.10 eV binding energies correspond to C 1s sp2, C 1s sp3 and C 1s C-O respectively.[35] As well Figure 4 b and c show a slight increase in the C 1s C-O band area from 3.92% to 5.34% after ball milling (FAC) proving the formation of new C-O functional groups on the surface of the activated carbon material.

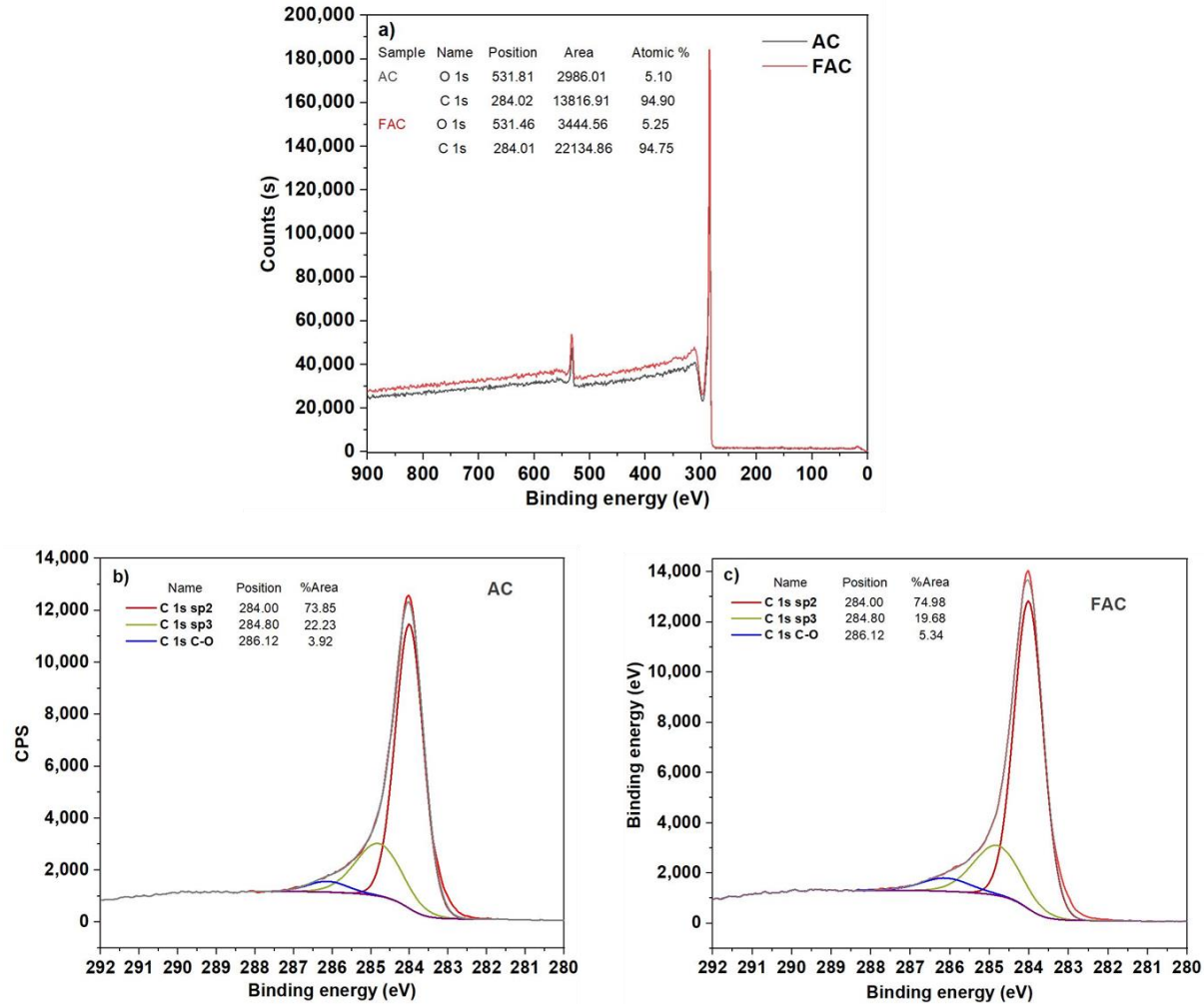

Figure 4: XPS complete survey of AC and FAC (a), deconvoluted XPS C 1s spectra of AC (b) and FAC (c)

3.3.2. Rheological properties and zeta potential: effect of particle distribution

To improve the flowing properties of carbon-based flowable electrodes in FCDI systems, bimodal distributions were used by mixing (different ratios) of FAC (size range: 0.3-0.6 µm) and AC (size range: 0.8-1.6 µm). This was based on the hypothesis that fine particles can fill the gaps between larger particles (packing effect), increasing the connectivity within the carbon network, while keeping enough free spaces for water to flow through (i.e. acceptable viscosity). The packing effect on the dynamic viscosity and surface charge (zeta potential) was studied first by measuring the viscosity in function of the shear rate and zeta potential of carbon suspensions with monomodal and bimodal distributions (different FAC to AC ratios) (Figure). The apparent viscosities of all carbon suspensions decreased when the applied shear rate was increased, showing a flow behavior typical of a pseudo-plastic fluid, this phenomenon is typical of non-Newtonian fluids.[36] Moreover, their viscosity (Figure 5(a)) increased proportionally with the FAC percentage. Upon dry ball grinding of AC, each particle is divided into many particles, thus increasing the particle number for the same weight percentage and flowable electrode volume. Consequently, the higher specific surface area of particles increases interactions with water, and dissipates more energy due to friction. This also

promotes particle-particle interactions, notably repulsion forces, leading to higher resistance to flow or higher viscosity. This is observed particularly at low shear rates.[37] This effect becomes less significant at higher shear rates because the interactive forces between particles are less effective. Moreover, wide and narrow particle size ranges are associated with low and high viscosity, respectively.[38] This explains the lower viscosity of AC samples because their particle size range was wider than that of FAC samples. Suspensions with wide particle size distribution (large polydispersity) aggregate more easily than suspensions with narrow polydispersity. This gives more of free space that facilitates the movement (flow) of individual particles, and thus lower viscosity. These results are in agreement with those by Harmadi *et al.*[39] and Buranasrisak *et al.*[40] who studied the particle size effect on the rheology and stability of carbon-water mixtures.

Zeta potentials represent the surface charge of particles in suspension. The particle size effects on zeta potential and apparent viscosity was studied**.** The electrostatic repulsive forces of particles in suspension under an applied voltage depend on their surface charge. It was found that zeta potential increases after ball-milling, which can be attributed to the increase in oxygenated functional groups on the surface of the material as shown previously in the XPS study. The addition of large particles with low zeta potential to the flow electrodes leads to decreased repulsive behavior, and decrease the suspension viscosity because the smaller specific surface area leads to less friction, as explained previously. However, suspensions of finer particles, which have strong surface charge (high zeta potential) increase particle-particle repulsion and the resistance to flow or viscosity. Similarly, zeta potential measurements (Figure (b)) showed the interdependence between viscosity, surface charge, and FAC percentage. As finer particles in suspension have stronger surface charge (higher zeta potential), particle-particle repulsion is promoted, decreasing aggregation. Consequently, the whole space is occupied by well-dispersed particles, and less space is available for free water flow, leading to higher viscosity. Upon reducing FAC percentage in the suspension, repulsion forces between particles were decreased as well as resistance to flow, and therefore, flowing behavior in the FCDI system was improved. These results are fully in line with those by Buranasrisak *et al.*[40].

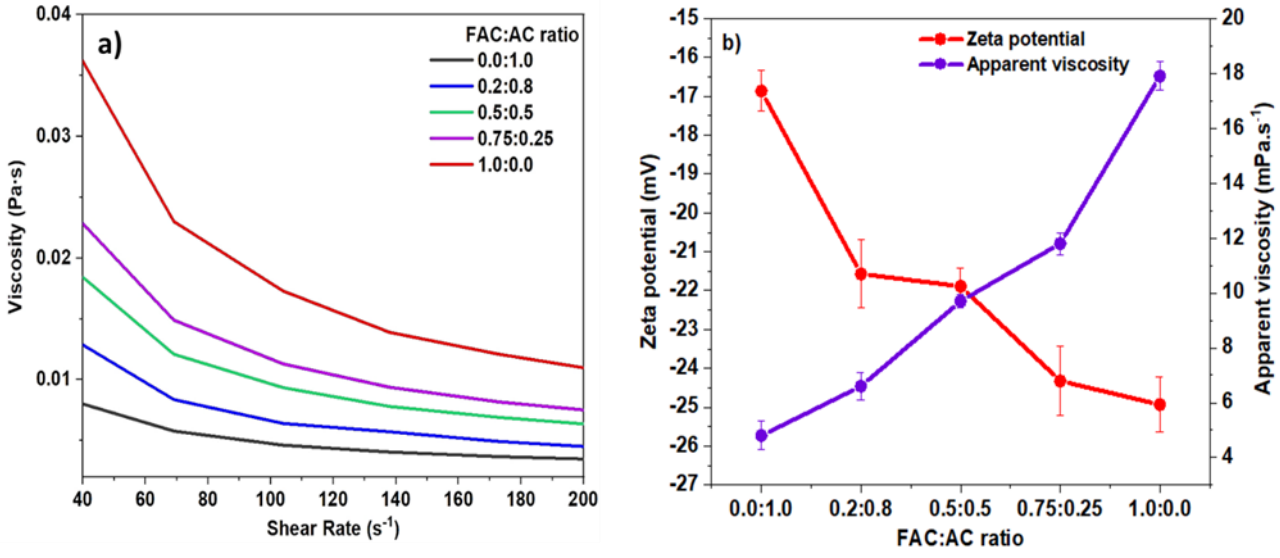

Figure 5: (a) Viscosity of carbon suspensions with different FAC to AC ratios at different shear rates. (b) Dependence of the apparent viscosity on zeta potential and fine particle (FAC) fraction (100rps

shear rate). All experiments were carried out with carbon suspensions with 10 % wt carbon loading, fine particle size range of 0.3-0.6 µm, and large particle size range of 0.8-1.6 µm.

3.3.3. Reynolds number

Reynolds number (i.e. the inertial forces to viscous forces ratio) is used to categorize the fluid systems where viscosity has an important effect in controlling the fluid velocity or flow pattern, a critical parameter in our study. For all mixtures, the Reynolds number (calculated using equation (5)) was <2100, indicating a laminar flow (i.e. the flow type needed for flowable electrodes in FCDI systems) (Table 2). As flow velocity is directly proportional to the Reynolds number, this explains the decrease of the Reynolds number in carbon suspensions with higher FAC percentages because they decrease the flow velocity. Consequently, when the viscosity increased with higher FAC: AC ratios, the Reynolds number decreased.

Table 2: Reynolds number of the indicated carbon suspensions

FAC : AC ratio	Reynolds n°
0.0 : 1.0	57.787 ± 0.006
0.2 : 0.8	45.033 ± 0.006
0.5 : 0.5	30.620 ± 0.001
0.75 : 0.25	21.808 ± 0.008
1.0 : 0.0	13.106 ± 0.030

3.3.4. *Physical stability*

AC particles suspended in water tend to settle due to gravitational force. In FCDI systems, this can cause clogging inside the channels, thus reducing the particle availability for ion adsorption during the process. The destabilization kinetics of suspensions with different fine to large particle ratios (at 10% wt) were evaluated by measuring the TSI (TURBISCAN® technology) over 30 minutes (**Erreur ! Source du renvoi introuvable.**). The TSI (i.e. destabilization) progressively increased for samples with lower FAC percentages. This indicates that the stability of the carbon suspensions increased with higher FAC percentages, although no difference was observed for samples with fine particles to large particle ratios of 0.75:0.25 and 1.0:0.0. Particle size reduction is associated with slower sedimentation rates. This is explained by the sedimentation velocity law shown in equation (6). Indeed, the particle size has an effect on the sedimentation velocity. According to Stokes' law, the particle sedimentation velocity is proportional to the density difference between the solid and liquid phase, inversely proportional to the fluid viscosity, and proportional to the particle diameter square. This explains the important decrease in sedimentation velocity with FAC percentage increase in the suspensions: smaller particle size is associated with higher viscosity. FAC particles remained in suspension and well dispersed for a longer period of time, thus increasing the intra-particle interactions in solution. These results are in agreement with the rheology and zeta potential data, and explain the behavior of the different carbon particle size suspensions as flowable electrodes.

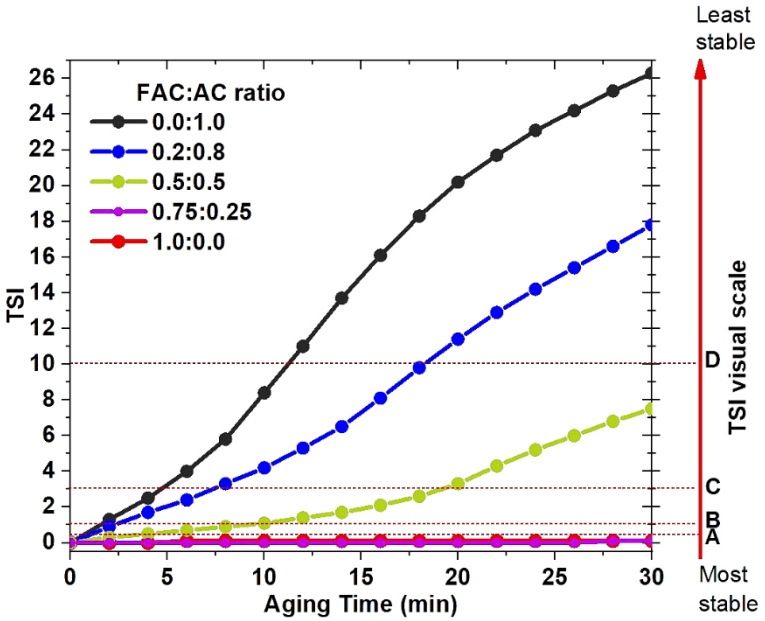

Figure 6: TURBISCAN® stability index (TSI) of the carbon suspensions at different ratios of fine particles to large particles. Below level A (lowest TSI dash line) on the TSI visual scale, no destabilization is observed. Level A marks the beginning of the very early destabilization stage. Level B indicates the beginning of destabilization, and levels C and D describe high sedimentation stages.

3.4. Electrochemical properties

To evaluate the electrochemical behavior of activated carbon electrodes with different FAC:AC ratios, cyclic voltammetry (CV) measurements were carried out using a 1 g/L NaCl electrolyte solution at 2 mV. s^{-1} scan rate with a -0.2 – 0.4 V voltage window. The CV results are shown in Figure 7 (a). All the electrodes displayed a symmetrical box-like shape, which reflects good capacitor characteristic. The larger area obtained under the CV curves implies the higher specific capacitance of the materials. The 1.0: 0.0 FAC: AC ratio (pure FAC) electrode showed the highest area obtained under the CV curves, indicating the highest specific capacitance compared to the pure AC electrode. As well, based on the cyclic voltammetry cycles, the EDL capacitance of the different electrodes of different FAC: AC ratios was calculated according to equation 8 and presented in figure 7 (b).[41] Thus, in all cases, the addition of FAC to the AC electrodes enhances their double layer capacitance due to the increased conductivity of the flow electrodes caused by the improved interconnectivity between the carbon particles in the case of FAC as explained in details before. Thus pure FAC electrode showed the highest specific capacitance of 35 $F.cm^{-2}$ compared to 25.5 $F.cm^{-2}$ in the case of pure AC marking a higher conductivity of FAC compared to AC.

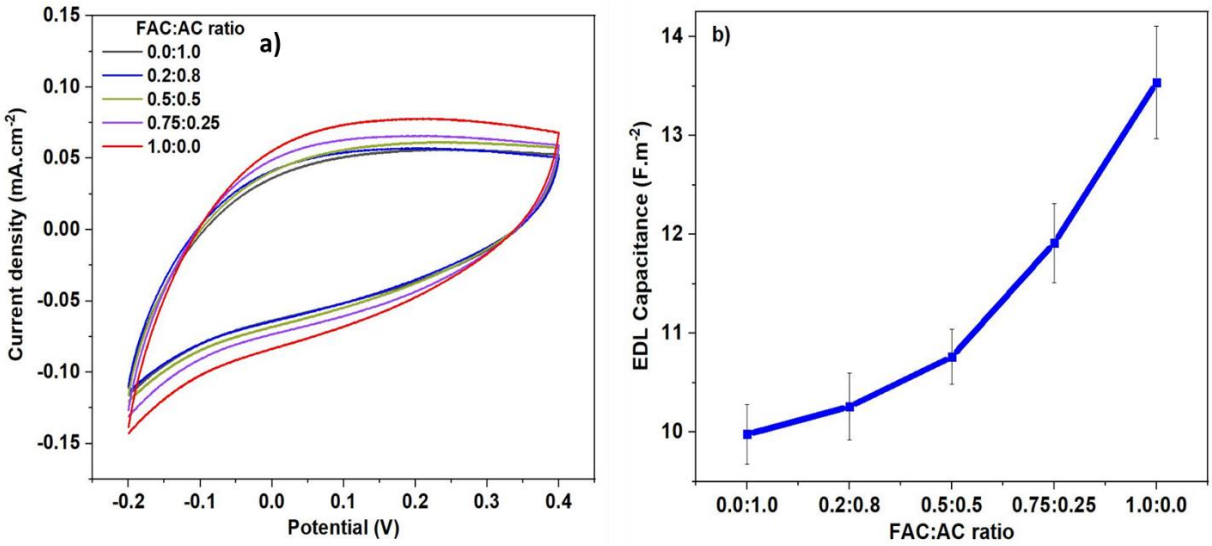

Figure 7: Cyclic voltammetry cycles (a) and electrical double layer capacitance (b) for activated carbon electrodes with different FAC:AC ratios.

3.5. Desalination performance

The electrosorption characteristics of the different carbon suspensions (10% wt carbon loading) as flow electrodes were investigated without clogging in our FCDI set-up. FCDI performance indicators (DE, SAC, SAR and CE) were calculated for the different mixtures (Table 3 and Figure (b and c)). In all cases, FAC addition strongly improved their salt adsorption capacity and desalination performance in FCDI. The higher specific surface area, more accessible pores, better conductivity observed upon particle size reduction explain the improved DE, SAC, and SAR values (Table 3, Figure 8 (b)). Higher surface area promotes mass transfer (ion adsorption), which is the limiting mass transfer phenomenon in FCDI. This strongly influences the SAR values, as seen after FAC addition in the flowable electrodes.

Sharper drop in ionic conductivity of the FS when using bimodal mixtures or pure FAC compared with pure AC was observed (Figure 7 (a)). Flowable electrodes with 0.75:0.25 and 1.0:0.0 FAC:AC ratios exhibited the best DE, the highest SAC and SAR among all samples (Table 3 Figure 8 (b and c)). DE was 72%, SAC was 32.3 $mg.g^{-1}$, and SAR was 1772 $\mu g.cm^{-2}.min^{-1}$ for the 0.75:0.25 sample compared with 34%, 15.3 $mg.g^{-1}$ and 839 $\mu g.cm^{-2}.min^{-1}$ for the pure AC flow electrode respectively. This can be due to the improved ion diffusion pathways within the carbon network because fine particles filled the void between larger particles, thus increasing contact areas within the carbon network, and consequently conductivity in the flowable electrode. The lower desalination performance of the flowable electrode with AC particles might be due to the lower repulsion forces between particles that aggregate to each other, thus masking the pores that become less accessible to ions. Furthermore, the higher resistance and lower conductivity caused by water occupying the large gaps between large AC particles create long ion diffusion pathways. These parameters explain the lower performance metrics of these flowable electrodes. The chronoamperometry curves (Figure S3 in SI) for the different carbon slurries showed the current density in function of time at a constant applied voltage (1V). Current density was lower for pure AC suspensions than for the samples with different FAC percentages. Therefore, the total charge transferred (which is the integration of the chronoamperometry curves) was lower for large AC particles, resulting in lower DE. The current density progressively increased with the percentage of FAC added, and

DE improved. Conversely, CE was comparable among samples (Figure 8 (c)), likely because this parameter is mostly influenced by the ion transfer through the selective IEM. For all samples, the same FCDI system with the same IEM was used, the conductivity of the saline solution passing between the electrodes was the same (5 g/L NaCl), and the quantity of carbon in the electrode compartments was largely enough to receive ions from the central compartment. The high selectivity of cationic and anionic membranes in such conditions explains the comparable CE values among samples.[42] Analysis of the relationship between the apparent viscosity and DE of the different flowable electrodes (Figure 8 (d)) showed that with the 0.75:0.25 FAC:AC ratio bimodal mixture, viscosity decreased by 30%, overcoming the major limitation of FAC-based flowable electrodes in FCDI (i.e. high viscosity). The challenge is always to find a compromise between these parameters to improve desalination performance in FCDI, while maintaining good flowing properties of the electrodes inside the system. In this study a good compromise between these parameters was achieved with the 0.75:0.25 FAC:AC ratio bimodal mixture.

Table 3: salt adsorption capacity (SAC) and average salt adsorption rate (SAR) of carbon flow electrodes with different FAC : AC ratio

FAC : AC ratio	SAC ($mg.g^{-1}$)	SAR ($\mu g.cm^{-2}.min^{-1}$)
0.0 : 1.0	15.3	0.51
0.2 : 0.8	27.6	0.92
0.5 : 0.5	28.9	0.96
0.75 : 0.25	32.3	1.08
1.0 : 0.0	31.9	1.06

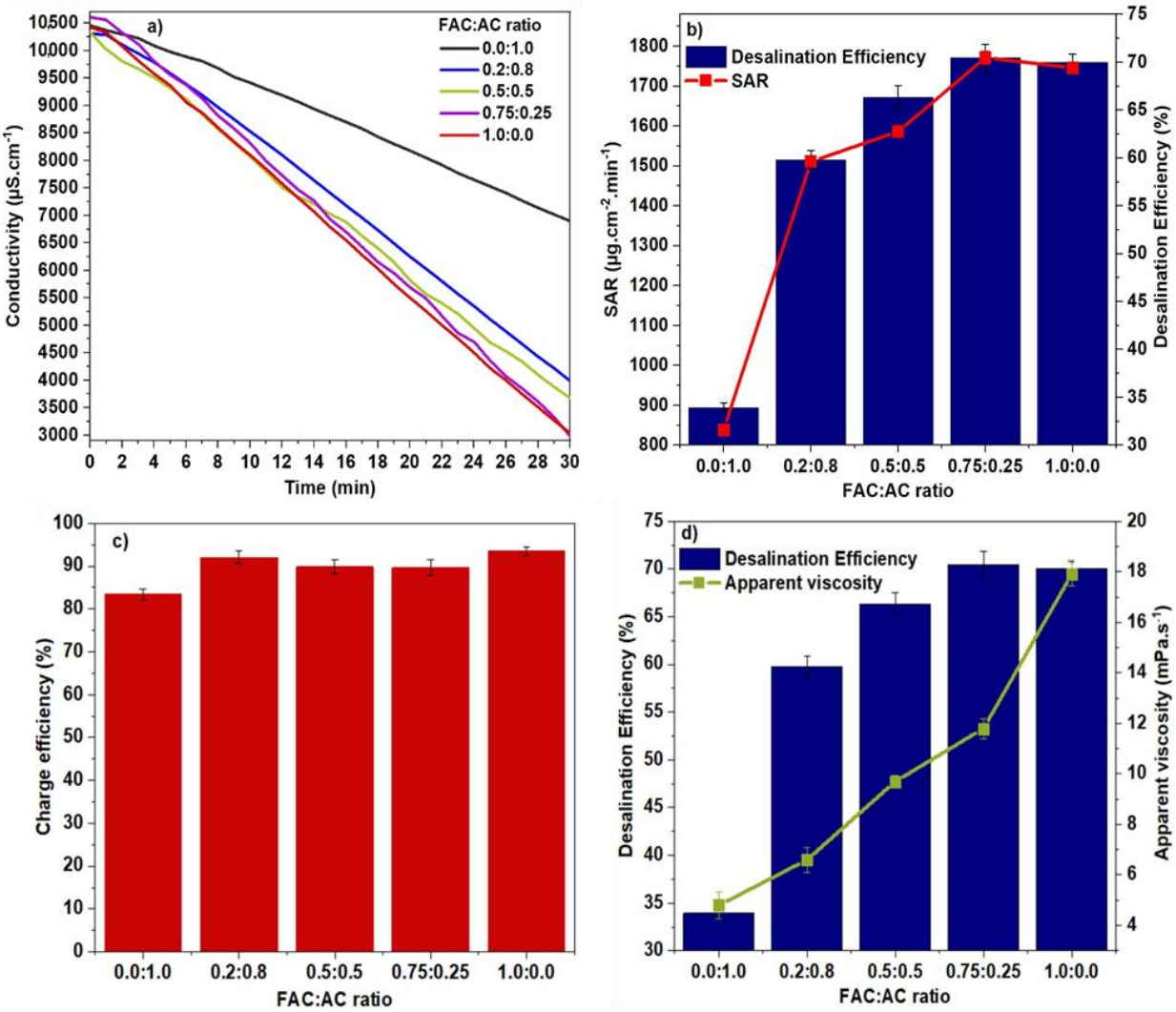

Figure 8: Feed solution conductivity (a), desalination efficiency and salt adsorption rate (SAR) (b), and charge efficiency (c) of carbon-based flowable electrodes with different FAC: AC ratios, during 30 min of FCDI experiment time. Relationship between desalination efficiency and apparent viscosity (d).

The rheological characteristics of the carbon slurries were studied to optimize their flowability inside the FCDI system because this has a direct effect on the pumping energy and cost. To this aim, viscosity effect on the pressure drop was assessed when comparing the desalination performances of the different flowable electrodes. In every FCDI process, there is always a compromise between particle size and viscosity. Smaller carbon particles increase conductivity, and consequently the process efficiency, for instance in terms of charge transfer, maximum salt capacity, mass transfer. However, adding small particles to the carbon slurry increases viscosity and also pumping costs due to the pressure drop increase. In our set-up, pressure drop (calculated with equation (7)) increased with the viscosity increase (Figure 9). With higher FAC percentages in the slurry, DE improved but viscosity increased, and also the pressure drop, leading to higher pumping energy and costs. Therefore, it is important to find the best compromise between particle size distribution and viscosity in order to obtain an energy-efficient process with good performance without clogging problems inside the FCDI system.

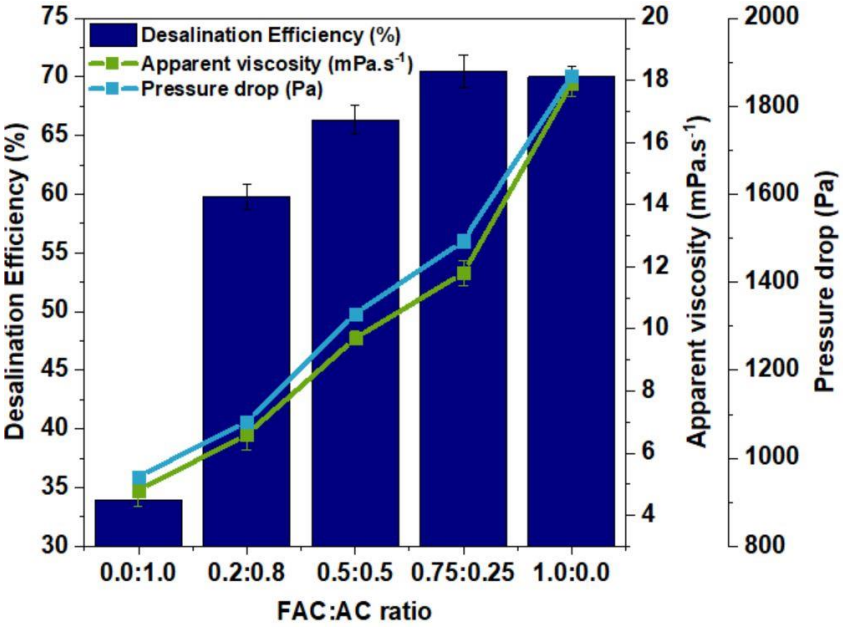

Figure 9: Relationship between desalination efficiency, apparent viscosity, and pressure drop increase of carbon-based flowable electrodes with the indicated FAC: AC ratios, during 30 min of FCDI experiment time.

4. Conclusion

This work investigated the effect of particle size distribution on the viscosity and desalination performance of AC-based flowable electrodes in FCDI. Mixtures of two different AC particle sizes were used: commercial AC and FAC obtained after ball-milling commercial AC. This experimental work shows that particle size distribution has a considerable effect on ion diffusion length and on the ion transport pathway that is determined by the packing density of flowable electrodes. Particularly, with pure AC suspensions, intraparticle and interparticle ion diffusion limited the desalination capacity (34% of DE). By mixing two different particle sizes, particle size distribution became broader, leading to better desalination performance, as indicated by the 72% of DE and improved flowing properties of the flowable electrode in FCDI (decrease by 33% of viscosity compared with the pure FAC suspension that achieved 70% of DE) in FCDI. These results highlighted the importance of particle size distribution and packing density on the behavior of flowable electrodes optimized for FCDI-based desalination. Fine particles and combined (0.75: 0.25 FAC: AC ratio) slurries showed better desalination performance compared to large particle slurries. However, large particle slurries showed better fluidity and easier flow in our water desalination system leading to lower pressure drop. Thus, good compromise must be done between high desalination capacity and acceptable pressure drop (viscosity) to have an optimal electrochemical desalination process. To find the best balance, more research is needed, including molecular dynamic simulations that can improve experimental procedures and save time.

Author Contributions: Conceptualization: M.T.; Methodology: M.B and M.C.; Formal analysis: M.T. S.L. and M.B. Investigation: M.T.; Resources: F.Z., M.B., P.S. and M.C.; Data

curation: M.T.; Original draft preparation: M.T.; Writing, review and editing: M.T., F.Z., M.B. and M.C.; Visualization: F.Z., M.T., M.B. and M.C.; Supervision: F.Z., M.B., P.S. and M.C.; Project administration: M.B., F.Z., P.S. and M.C. All authors have read and agreed to the published version of the manuscript.

Conflicts of Interest: The authors declare no conflict of interest.

References

1. Folaranmi, G. *et al.* Towards Electrochemical Water Desalination Techniques: A Review on Capacitive Deionization, Membrane Capacitive Deionization and Flow Capacitive Deionization. *Membranes* **10**, E96 (2020).
2. Jeon, S. *et al.* Desalination via a new membrane capacitive deionization process utilizing flow-electrodes. *Energy Environ. Sci.* **6**, 1471–1475 (2013).
3. Seo, S.-J. *et al.* Investigation on removal of hardness ions by capacitive deionization (CDI) for water softening applications. *Water Res.* **44**, 2267–2275 (2010).
4. Kalfa, A. *et al.* Capacitive deionization for wastewater treatment: Opportunities and challenges. *Chemosphere* **241**, 125003 (2020).
5. Porada, S. *et al.* Review on the science and technology of water desalination by capacitive deionization. *Prog. Mater. Sci.* **58**, 1388–1442 (2013).
6. Lee, J.-B. *et al*. Desalination of a thermal power plant wastewater by membrane capacitive deionization. *Desalination* **196**, 125–134 (2006).
7. Andelman, M. D. *et al*. Charge barrier flow-through capacitor. (2004).
8. Biesheuvel, P. M. *et al*. Theory of membrane capacitive deionization including the effect of the electrode pore space. *J. Colloid Interface Sci.* **360**, 239–248 (2011).

9. Zhang, C. *et al.* Flow Electrode Capacitive Deionization (FCDI): Recent Developments, Environmental Applications, and Future Perspectives. *Environ. Sci. Technol.* **55**, 4243–4267 (2021).
10. Presser, V. *et al.* The Electrochemical Flow Capacitor: A New Concept for Rapid Energy Storage and Recovery. *Adv. Energy Mater.* **2**, 895–902 (2012).
11. Tang, K. *et al*. Optimal conditions for efficient flow-electrode capacitive deionization. *Sep. Purif. Technol.* **240**, 116626 (2020).
12. Liu, Z. *et al*. A Brief Review on High-Performance Capacitive Deionization Enabled by Intercalation Electrodes. *Glob. Chall.* **5**, 2000054 (2021).
13. Ma, J. *et al.* Flow-electrode capacitive deionization (FCDI) scale-up using a membrane stack configuration. *Water Res.* **168**, 115186 (2020).
14. Tang, K. *et al*. Water Desalination by Flow-Electrode Capacitive Deionization in Overlimiting Current Regimes. *Environ. Sci. Technol.* **54**, 5853–5863 (2020).
15. Shi, W. *et al.* Exploration of Energy Storage Materials for Water Desalination via Next-Generation Capacitive Deionization. *Front. Chem.* **8**, 415 (2020).
16. Ryoo, M.-W. *el al*. Improvement in capacitive deionization function of activated carbon cloth by titania modification. *Water Res.* **37**, 1527–1534 (2003).
17. Hou, C.-H. *et al*. Development of multi-walled carbon nanotube/poly(vinyl alcohol) composite as electrode for capacitive deionization. *Sep. Purif. Technol.* **130**, 7–14 (2014).
18. El-Deen, A. *et al*. Graphene wrapped MnO2-nanostructures as effective and stable electrode materials for capacitive deionization desalination technology. *Desalination* **344**, 289–298 (2014).
19. Liu, X. *et al*. Fabrication of graphene/activated carbon nanofiber composites for high performance capacitive deionization. *J. Taiwan Inst. Chem. Eng.* **72**, 213–219 (2017).
20. Park, K.-K. *et al.* Development of a carbon sheet electrode for electrosorption desalination. *Desalination* **206**, 86–91 (2007).

21. Cheng, Y. *et al.* A review of modification of carbon electrode material in capacitive deionization. *RSC Adv.* **9**, 24401–24419 (2019).
22. Zhao, X. *et al*. Electrode materials for capacitive deionization: A review. *J. Electroanal. Chem.* **873**, 114416 (2020).
23. Huang, K. *et al.* Significantly increasing porosity of mesoporous carbon by NaNH2 activation for enhanced CO2 adsorption. *Microporous Mesoporous Mater.* **230**, (2016).
24. Teng, H. *et al*. High-Porosity Carbons Prepared from Bituminous Coal with Potassium Hydroxide Activation. *Ind. Eng. Chem. Res.* **38**, 2947–2953 (1999).
25. Zhang, H. *et al.* Constructing Hierarchical Porous Carbons With Interconnected Micro-mesopores for Enhanced CO2 Adsorption. *Front. Chem.* **7**, (2020).
26. Zhang, Y. *et al*. Particle size distribution influence on capacitive deionization: Insights for electrode preparation. *Desalination* **525**, 115503 (2022).
27. Cohen, H. *et al*. E. Suspension Electrodes Combining Slurries and Upflow Fluidized Beds. *ChemSusChem* **9**, 3045–3048 (2016).
28. Folaranmi, G. *et al.* Investigation of fine activated carbon as a viable flow electrode in capacitive deionization. *Desalination* **525**, 115500 (2022).
29. Jung, Y. *et al.* Enhanced Electrochemical Stability of a Zwitterionic-Polymer-Functionalized Electrode for Capacitive Deionization. *ACS Appl. Mater. Interfaces* **10**, 6207–6217 (2018).
30. Zhao, R. *et al*. Optimization of salt adsorption rate in membrane capacitive deionization. *Water Res.* **47**, 1941–1952 (2013).
31. Porada, S. *et al.* Direct prediction of the desalination performance of porous carbon electrodes for capacitive deionization. *Energy Environ. Sci.* **6**, 3700–3712 (2013).
32. Bridges, S. *et al*. Chapter 1 - Rheology. in *A Practical Handbook for Drilling Fluids Processing* (eds. Bridges, S. & Robinson, L.) 3–26 (Gulf Professional Publishing, 2020).

33. Meister, F. *et al.* 6 - Additional clinical applications. in *Artificial Intelligence for Computational Modeling of the Heart* (eds. Mansi, T., Passerini, T. & Comaniciu, D.) 183–210 (Academic Press, 2020). doi:10.1016/B978-0-12-817594-1.00017-6.
34. Chandra, S. *et al.* Molecular Level Control of the Capacitance of Two-Dimensional Covalent Organic Frameworks: Role of Hydrogen Bonding in Energy Storage Materials. *Chem. Mater.* **29**, 2074–2080 (2017).
35. Rossin, J. A. XPS surface studies of activated carbon. *Carbon* **27**, 611–613 (1989).
36. Poslinski, A. J. *et al*. Rheological Behavior of Filled Polymeric Systems I. Yield Stress and Shear-Thinning Effects. *J. Rheol.* **32**, 703–735 (1988).
37. Hou, H. *et al*. Quantifying effects of particulate properties on powder flow properties using a ring shear tester. *J. Pharm. Sci.* **97**, 4030–4039 (2008).
38. Barthelmes, G. *et al*. Particle size distributions and viscosity of suspensions undergoing shear-induced coagulation and fragmentation. *Chem. Eng. Sci.* **58**, 2893–2902 (2003).
39. Harmadi, E. *et al*. Effect of Particle Size Distribution on Rheology and Stability of High Concentration Coal-Water Mixture (Cwm) With Indonesian Low Rank Coal. *undefined* (2009).
40. Buranasrisak, P. *et al*. Effects of Particle Size Distribution and Packing Characteristics on the Preparation of Highly-Loaded Coal-Water Slurry. *Int. J. Chem. Eng. Appl.* **3**, 31–35 (2012).
41. Jiménez, M. L. *et al.* Multiionic effects on the capacitance of porous electrodes. *Phys. Chem. Chem. Phys.* **20**, 5012–5020 (2018).
42. Pismenskaya, N. *et al.* A Review on Ion-Exchange Membranes Fouling during Electrodialysis Process in Food Industry, Part 2: Influence on Transport Properties and Electrochemical Characteristics, Cleaning and Its Consequences. *Membranes* **11**, 811 (2021).